



Prediction of oxygen ion conduction from relative Coulomb electronic interactions in oxyapatites

Yingzhi Zeng^a, Pei-Lin Mao^b, San Ping Jiang^c, Pearson Wu^b, Lan Zhang^c, Ping Wu^{a,*}

^a Institute of High Performance Computing, 1 Fusionopolis Way, #16-16 Connexis, Singapore 138632, Singapore

^b School of Chemical & Life Sciences, Nanyang Polytechnic, 180 Ang Mo Kio Avenue 8, Singapore 569830, Singapore

^c Fuel Cells Strategic Research Program, School of Mechanical & Aerospace Engineering, Division of Manufacturing Engineering, Nanyang Technological University, 50 Nanyang Avenue, Singapore 639798, Singapore

ARTICLE INFO

Article history:

Received 24 September 2010

Received in revised form

14 December 2010

Accepted 2 January 2011

Available online 19 January 2011

Keywords:

Solid oxide fuel cell

Apatite structure

Coulomb energy

Ionic conductivity

Modelling

ABSTRACT

In order to offer a guideline to search for new oxyapatites exhibiting high ionic conductivities (σ) for possible application in solid oxide fuel cells operating at intermediate temperatures (IT-SOFCs), a mathematical model is developed, i.e., a linear relation of σ and the relative Coulomb energy, to predict the σ of oxyapatites. The inputs to the model are two readily available elemental properties, namely the ionic radius and the electronegativity of the constituent elements. The model not only predicts the ionic conductivities of 45 oxyapatites but also rationalizes the observed trends reported in the literatures. The effects of the two elemental properties on ionic conductivity are also examined and predict a wide range of new oxygen stoichiometric oxyapatites with ionic conductivities potentially as high as 10^{-2} – 10^{-1} S cm⁻¹ at 500 °C is predicted. The investigations suggest an optimization strategy to search for promising oxyapatites, i.e., applying dopants with large ionic radii and low electronegativities.

© 2011 Elsevier B.V. All rights reserved.

1. Introduction

Materials with high ionic conductivities have attracted widespread interest due to their possible application in many areas such as solid oxide fuel cells (SOFCs), oxygen sensors and separation membranes [1–4]. Ytria stabilized zirconia (YSZ) is the most favoured SOFC electrolyte due to its high oxygen ionic conductivity and structural stability at elevated temperatures (900–1000 °C). On reducing the operating temperature of a SOFC to intermediate values of 600–800 °C (IT-SOFCs), however, the ionic conductivity of YSZ decreases significantly [2]. Thus, to overcome the disadvantages arising from a reduced operating temperature, great efforts have been made to search for other oxygen ion conductors with high ionic conductivity at lower temperatures (600–800 °C) [1,5]. Among them, an apatite-type oxygen ion conductor based on lanthanum silicate, La_{9.33}Si₆O₂₆, shows significant promise as an electrolyte for IT-SOFCs [1–19]. It has been reported [4] that the conductivities of La_{9.33}Si₆O₂₆ are 1.1×10^{-4} and 2×10^{-3} S cm⁻¹ at 500 and 800 °C, respectively.

The structure of a typical oxyapatite consists of isolated SiO₄ tetrahedral units and rare earth cations located in 9 coordinate (La1/La2) and 7 coordinate (La3) channel sites [20]. The remaining oxygen ions occupy one-dimensional channels running through the structure, which are considered as vital for high oxygen ion conduction in such materials [21]. Both experimental and theoretical evidence indicate that oxyapatites conduct ions via an interstitial mechanism [1,7,22], and local cooperative relaxation of SiO₄ tetrahedra is an important factor for facile oxygen ion conduction. In other words, Si and the nearest oxygen ions generally displace away from the channel and towards the La1/La2 sites, as suggested by the observed changes in ionic conductivity of Mg-doped La_{9.33}(SiO₄)₆O₂ [23]. A large enhancement in conductivity was observed when Mg was doped on the Si sites, whereas the conductivity decreased when Mg was doped on La sites [23]. This suggests that Mg leads to a local expansion of the channels when it is on Si sites, while it encroaches the oxygen ion channels when it is doped on La sites. Further studies revealed that non-stoichiometry and partial occupancy on the La1/La2 sites have the same effect on the conductivity as the incorporation of excess oxygen into the system [8]. Also, it was reported that a wide range of cation substitutions in an oxyapatite are possible due to the flexibility of the apatite structure in accommodating a range of ion sizes, and this enhances the success in searching for new oxyapatites of high ionic conductivity.

* Corresponding author. Tel.: +65 64191212; fax: +65 64632536.

E-mail addresses: zengyz@ihpc.a-star.edu.sg (Y. Zeng), Peilin.mao@yahoo.com (P.-L. Mao), S.Jiang@curtin.edu.au (S.P. Jiang), pearsonvip@hotmail.com (P. Wu), ZhangLan@ntu.edu.sg (L. Zhang), wuping@ihpc.a-star.edu.sg (P. Wu).

Inspired by the above findings from experimental and theoretical investigations, a mathematical model is proposed in this study to predict the ionic conductivities of oxyapatites in an attempt to provide a guideline to search for, or synthesize, new oxyapatites. As an initial attempt, only oxygen stoichiometric oxyapatites are considered. In the model, it is postulated that the expansion of c-axis channels plays a central role in the enhancement of oxygen ion conduction and the Coulomb interaction between two charged units of SiO_4 tetrahedra and a La1/La2 site dominates the expansion or contraction of c-axis channels. The interaction energy, i.e., the relative Coulomb energy, is formulated by a set of variables that are properly defined in terms of two fundamental properties of the constituent elements (i.e., electronegativity and ionic radius) and composition. According by, a linear relation between the relative Coulomb energies and the logarithmic ionic conductivities is established. This linear relation is examined for 45 oxygen stoichiometric oxyapatite compositions reported in the literature, and a good correlation with the coefficient of determination $R^2 = 0.81$ is achieved. Since the inputs to the model, namely, the fundamental properties of elements, are readily available, the model enables the evaluation or prediction of the conductivities for a large number of oxyapatites with much less computation effort. The effects of ionic radius and electronegativity on ionic conductivity are discussed on the basis of the model. An examination is also made of oxyapatites that are virtually generated by numerically substituting a range of elements into the Si and La1/La2 sites, respectively. New oxyapatites with high conductivities from 10^{-2} to $10^{-1} \text{ S cm}^{-1}$ at 500°C are predicted.

2. Model development

Oxygen stoichiometric apatite oxides have the general formula $\text{A}_{10-x}(\text{BO}_4)_6\text{O}_2$ where A and B are a range of cations, e.g., A is a rare-earth or alkaline-earth element, and B is Si or Ge, etc. The structure of the typical oxyapatite $\text{La}_{9.33}\text{Si}_6\text{O}_{26}$ is hexagonal in symmetry where the B cations (Si) take tetrahedral coordination with the structural oxygen (SiO_4), whereas the A cations (La) locate in seven- (La3) and nine-coordinate (La1/La2) cavity sites. The nine-coordinate position lies in the centre of the smaller of the two structural channels, and the seven-coordinate position lies around the periphery of the larger channel in the centre of which reside oxygen ions. The extra oxygen ions occupy the larger channels running along the c-axis, which are responsible for the high oxygen ion conductivity [14–16].

As stated in [24], lanthanum atoms usually fully occupy La3 sites, while cationic vacancies are randomly distributed on La1/La2 sites where rare-earth and alkaline-earth elements can be doped. Therefore, the interaction between the SiO_4 tetrahedra and La1/La2 site is postulated to be dominant for the expansion or contraction of the c-axis channel. In this study, the interaction is represented by a relative Coulomb energy between the two charged sites of A (La1/La2) and B (SiO_4), as illustrated in Fig. 1. On the other hand, the Coulomb interaction between the SiO_4 tetrahedra and a La3 site is secondary since, in most cases, the La3 site remains intact when the chemistry of an oxyapatite is changed. In another words, the SiO_4 tetrahedra/La3 interaction forms a common reference.

The A and B sites are taken as two circles as shown in Fig. 2. The relative Coulomb energy between the two sites is formulated by two-dimensional integration of the charge densities of the two sites. The derivation starts from the classic Coulomb energy, as defined by Eq. (1) where q_A and q_B are charges of A and B sites, respectively, and r and k_e denote the distance between the centres of the two sites and the Coulomb constant, respectively.

$$E = k_e \frac{q_A q_B}{r} \quad (1)$$

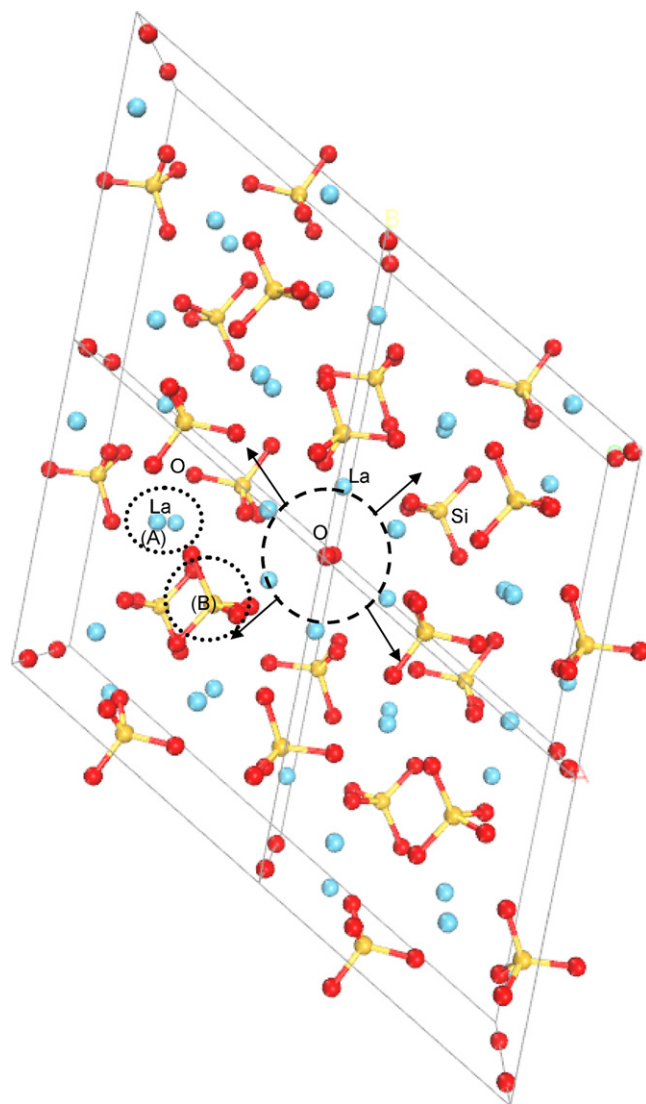


Fig. 1. Two charged units in structure of $\text{La}_{9.33}\text{Si}_6\text{O}_{26}$ (viewed from c-axis): (A)—La1/La2; (B)—tetrahedral (SiO_4).

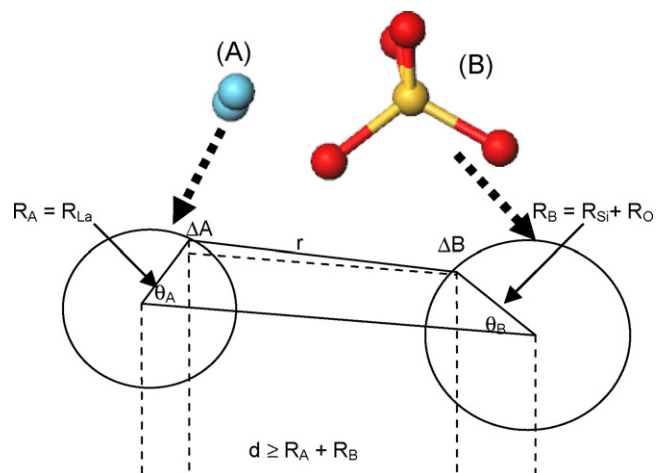


Fig. 2. Schematic diagram of A and B sites of $\text{La}_{9.33}\text{Si}_6\text{O}_{26}$.

The Coulomb energy is evaluated by assuming that the charge densities of the two units are uniformly distributed along the peripheries of A and B, respectively. The charges of two infinitesimals of circles A and B, i.e., ΔA and ΔB , are evaluated as Eqs. (2)–(3) where ρ_A and ρ_B are the charge densities of the peripheries of A and B, and R_A and R_B are the ionic radii of A and B, respectively. It is noted that R_B is the sum of the radii of Si^{4+} and O^{2-} .

$$\Delta q_A = \rho_A R_A d\theta_A \quad (2)$$

$$\Delta q_B = \rho_B R_B d\theta_B \quad (3)$$

The distance between the two infinitesimals on circles A and B, denoted as r , is evaluated as:

$$r^2 = c(1 + a \sin \theta_B + b \cos \theta_B) \quad (4)$$

where

$$a = \frac{-2R_A R_B \sin \theta_A}{R_A^2 + R_B^2 + d^2 - 2dR_A \cos \theta_A} \quad (5)$$

$$b = \frac{-2R_B(d - R_A \cos \theta_A)}{R_A^2 + R_B^2 + d^2 - 2dR_A \cos \theta_A} \quad (6)$$

$$c = R_A^2 + R_B^2 + d^2 - 2dR_A \cos \theta_A \quad (7)$$

The Coulomb energy between circle A and circle B can be evaluated by taking the double integrations as Eq. (8).

$$E_{A-B} = \rho_A \rho_B R_A R_B \int_0^{2\pi} \int_0^{2\pi} \frac{1}{r} d\theta_B d\theta_A \quad (8)$$

Substituting r (defined in Eq. (4)) into Eq. (8) yields:

$$E_{A-B} = \rho_A \rho_B R_A R_B \int_0^{2\pi} \frac{1}{\sqrt{c}} d\theta_A \int_\alpha^{2\pi+\alpha} \frac{1}{\sqrt{1 + \sin \theta}} d\theta \quad (8a)$$

where $\alpha = \arctan(a/b)$ and $\theta = \alpha + \theta_B$. Let $\gamma = \int_\alpha^{2\pi+\alpha} \frac{1}{\sqrt{1 + \sin \theta}} d\theta$ and note that γ turns out to be a constant. Substitution of c and γ into Eq. (8a) gives:

$$E_{A-B} = \frac{\gamma \rho_A \rho_B R_A R_B}{\sqrt{R_A^2 + R_B^2 + d^2}} \int_0^{2\pi} \frac{1}{\sqrt{1 + \xi \cos \theta_A}} d\theta_A \quad (8b)$$

where

$$\xi = \frac{-2dR_A}{R_A^2 + R_B^2 + d^2} \quad (9)$$

Let $Z = \int_0^{2\pi} \frac{1}{\sqrt{1 + \xi \cos \theta_A}} d\theta_A$ and then Eq. (8b) is reduced:

$$E_{A-B} = \frac{\gamma Z \rho_A \rho_B R_A R_B}{\sqrt{R_A^2 + R_B^2 + d^2}} \quad (8c)$$

In this work, the charge density ρ and the circle radius are associated with the electronegativities and ionic radii of the constituent elements, respectively. Both electronegativity and ionic radius are fundamental elemental properties. The resultant Coulomb energy E_{A-B} is thus a relative quantity. To establish the relationship between the relative Coulomb energy and the ionic conductivity with acceptable accuracy, the charge densities and ionic radii in Eq. (8c) are re-defined with the properties of La and Si as the reference in the following section.

The general formula of an oxygen stoichiometric oxyapatite with dopants is given as $A1_{a1}A2_{a2}B1_{b1}B2_{b2}B3_{b3}O_{26}$ where the A and B sites are occupied by up to two and three types of cation, respectively. In particular, A1 is occupied by trivalent cations only and A2 can be occupied by divalent or trivalent cations; B1 is occupied by tetravalent cations only, while B2 and B3 can be occupied by either divalent or trivalent cations.

Table 1
Elemental properties of ions.

Element	Charge	Ionic radius (Å)	Electro-negativity
Al	3+	0.54	1.61
B	3+	0.23	2.04
Ba	2+	1.35	0.89
Ca	2+	1	1.00
Co	3+	0.55	1.88
Eu	3+	0.95	1.12
Fe	3+	0.55	1.83
Ga	3+	0.62	1.81
Gd	3+	0.94	1.20
Ge	4+	0.53	2.01
La	3+	1.03	1.10
Mg	2+	0.72	1.31
Nd	3+	0.98	1.14
O	2-	1.4	3.44
Pr	3+	0.99	1.13
Si	3+	0.4	1.90
Sm	3+	0.96	1.17
Sr	2+	1.18	0.95
Zn	2+	0.74	1.65

The subscripts $a1$, $a2$, $b1$, $b2$ and $b3$ designate the compositions of the associated elements, and the total number of cations is summed up as $N = a1 + a2 + b1 + b2 + b3$. The average charges of A and B sites are calculated as Eqs. (10) and (11), respectively.

$$n_A^{avg} = x n_{A1} + (1 - x) n_{A2} \quad (10)$$

$$n_B^{avg} = y_1 n_{B1} + y_2 n_{B2} + (1 - y_1 - y_2) n_{B3} \quad (11)$$

where n_{A1} , n_{A2} , n_{B1} , n_{B2} and n_{B3} are the valences of cations A1, A2, B1, B2 and B3, respectively; x , y_1 , and y_2 are normalized compositions, i.e., $x = a1/(a1 + a2)$, $y_1 = b1/(b1 + b2 + b3)$, $y_2 = b2/(b1 + b2 + b3)$. The superscript 'avg' denotes the average values.

The average ionic radius of the A site is evaluated in terms of the radii of A1 and A2. Since A1 can only be occupied by trivalent cations, its radius remains unchanged and is denoted by the superscript 'org'. On the other hand, A2 can be occupied by divalent or trivalent cations, its radius is thus modified as Eq. (12) and denoted by the superscript 'mod'. Specifically, the A2 original radius is multiplied by a factor defined as the valence ratio of A2 to La^{3+} (=3).

$$R_{A2}^{mod} = \frac{n_{A2}}{3} R_{A2}^{org} \quad (12)$$

The average radius of the A site is defined as:

$$R_A^{avg} = x R_{A1}^{org} + (1 - x) R_{A2}^{mod} \quad (13)$$

The ionic radii of B2 and B3 are modified in terms of the Si valence, n_{Si} (=4), and the coordination numbers of Si^{4+} (=4) and La^{3+} (=9).

$$R_{B2}^{mod} = \frac{n_{B2}}{n_{\text{Si}}} \times \frac{9}{4} \times R_{B2}^{org} = \frac{9}{16} n_{B2} R_{B2}^{org} \quad (14)$$

$$R_{B3}^{mod} = \frac{n_{B3}}{n_{\text{Si}}} \times \frac{9}{4} \times R_{B3}^{org} = \frac{9}{16} n_{B3} R_{B3}^{org} \quad (15)$$

The original radius of B1 is used without any modification as B1 can only be occupied by tetravalent cations. The average radius of the B site is thus obtained in the similar fashion as that of the A site, namely:

$$R_B^{avg} = y_1 R_{B1}^{org} + y_2 R_{B2}^{mod} + (1 - y_1 - y_2) R_{B3}^{mod} \quad (16)$$

The distance between the centres of A and B sites can be represented as the sum of the average radii of the A site and B site, multiplied by a constant λ (>0), i.e.,

$$d = \lambda (R_A^{avg} + R_B^{avg} + R_O^{org}) \quad (17)$$

Table 2
Reported oxyapatite ionic conductivities at 500 °C.

No.	Oxyapatite	Conductivity, σ (S cm ⁻¹)	References
1	Pr _{9.33} Si ₆ O ₂₆	8.10×10^{-5}	Table 1 in [2]
2	La _{9.33} Si ₆ O ₂₆	1.10×10^{-4}	
3	Nd _{9.33} Si ₆ O ₂₆	1.00×10^{-4}	
4	Sm _{9.33} Si ₆ O ₂₆	2.20×10^{-5}	
5	Gd _{9.33} Si ₆ O ₂₆	1.50×10^{-6}	
6	La _{8.67} BaSi ₆ O ₂₆	1.40×10^{-4}	
7	La _{8.33} Ba _{1.5} Si ₆ O ₂₆	6.60×10^{-5}	
8	La _{8.67} SrSi ₆ O ₂₆	8.30×10^{-5}	
9	La _{8.33} Sr _{1.5} Si ₆ O ₂₆	1.30×10^{-5}	
10	La _{8.67} CaSi ₆ O ₂₆	5.80×10^{-5}	
11	La _{8.33} Ca _{1.5} Si ₆ O ₂₆	3.40×10^{-5}	
12	La _{9.5} Si _{5.5} Ga _{0.5} O ₂₆	4.60×10^{-4}	
13	La _{9.67} Si ₅ GaO ₂₆	1.00×10^{-3}	
14	La _{9.83} Si _{4.5} Ga _{1.5} O ₂₆	1.30×10^{-3}	
16	La _{9.5} Si _{5.5} B _{0.5} O ₂₆	4.10×10^{-4}	
17	La _{9.67} Si ₅ BO ₂₆	3.30×10^{-4}	
18	La _{9.83} Si _{4.5} B _{1.5} O ₂₆	4.90×10^{-4}	
19	La ₉ Mg _{0.5} Si ₆ O ₂₆	2.10×10^{-5}	
20	La _{8.67} MgSi ₆ O ₂₆	3.60×10^{-6}	
21	La _{9.33} Mg _{0.5} Si _{5.5} Mg _{0.5} O ₂₆	1.60×10^{-4}	
22	La _{9.5} Si _{5.75} Mg _{0.25} O ₂₆	1.80×10^{-3}	
23	La _{9.67} Si _{5.5} Mg _{0.5} O ₂₆	3.00×10^{-3}	
24	La _{9.5} Si _{5.75} Zn _{0.25} O ₂₆	2.10×10^{-3}	
25	La _{9.33} Ba _{0.5} Si _{5.5} Mg _{0.5} O ₂₆	1.80×10^{-3}	Table 3 in [9]
26	La _{9.83} Si ₅ Mg _{0.5} B _{0.5} O ₂₆	1.90×10^{-3}	
27	La _{9.83} Si ₅ Mg _{0.5} Ga _{0.5} O ₂₆	3.10×10^{-3}	
28	Eu _{9.33} Si ₆ O ₂₆	1.30×10^{-5}	Table 4a in [9]
29	Pr _{9.67} Si ₅ GaO ₂₆	1.10×10^{-4}	Table 4b in [9]
30	Nd _{9.67} Si ₅ GaO ₂₆	1.50×10^{-5}	
31	Sm _{9.67} Si ₅ GaO ₂₆	7.60×10^{-6}	
32	Eu _{9.67} Si ₅ GaO ₂₆	7.20×10^{-6}	
33	Gd _{9.67} Si ₅ GaO ₂₆	1.20×10^{-6}	
34	La _{9.83} Si _{4.5} Fe _{1.5} O ₂₆	1.26×10^{-4}	Fig. 10 in [11]
35	La _{6.83} Pr ₃ Si _{4.5} Fe _{1.5} O ₂₆	1.00×10^{-4}	
36	La _{3.83} Pr ₆ Si _{4.5} Fe _{1.5} O ₂₆	1.00×10^{-4}	
37	La _{9.83} Si _{4.5} Al _{1.5} O ₂₆	1.00×10^{-3}	
38	La _{9.83} Si _{4.5} AlFe _{0.5} O ₂₆	2.51×10^{-4}	Fig.3 in [10]
39	La _{9.83} Si _{4.5} Al _{0.5} FeO ₂₆	1.26×10^{-4}	
40	La _{9.67} Si ₅ FeO ₂₆	1.03×10^{-4}	Fig. 2 in [8]
41	La _{9.83} Si _{4.5} Co _{1.5} O ₂₆	8.16×10^{-4}	Fig. 4 in [8]
42	La _{9.67} Si ₅ CoO ₂₆	5.15×10^{-4}	
43	La _{8.5} Sr _{1.5} Si _{5.5} Al _{0.5} O ₂₆	8.20×10^{-6}	Table 1 in [12]
44	La _{9.5} Si _{5.5} Al _{0.5} O ₂₆	1.70×10^{-4}	
45	La _{9.33} Ge ₆ O ₂₆	1.12×10^{-4}	Fig. 4 in [13]

Eq. (9) can thus be rewritten as:

$$\xi = \frac{-2dR_A^{avg}}{(R_A^{avg})^2 + (R_B^{avg} + R_O^{org})^2 + d^2} \quad (9a)$$

Next, the electronegativities of the A and B the sites are modified as represented by Eqs. (18)–(19), where E_M^{org} ($M=A1, A2, B1, B2, B3$) denotes the original electronegativity of the corresponding cation.

$$E_A^{mod} = xE_{A1}^{org}(R_{A1}^{org})^{0.6} + (1-x)E_{A2}^{org}(R_{A2}^{mod})^{0.6} \quad (18)$$

$$E_B^{mod} = y_1E_{B1}^{org}(R_{B1}^{org})^{0.6} + y_2E_{B2}^{org}(R_{B2}^{mod})^{0.6} + (1-y_1-y_2)E_{B3}^{org}(R_{B3}^{mod})^{0.6} \quad (19)$$

Similarly, the modified electronegativities of O²⁻ and La³⁺ are evaluated as Eqs. (20) and (21), respectively.

$$E_O^{mod} = E_O^{org}(R_O^{org})^{0.6} \quad (20)$$

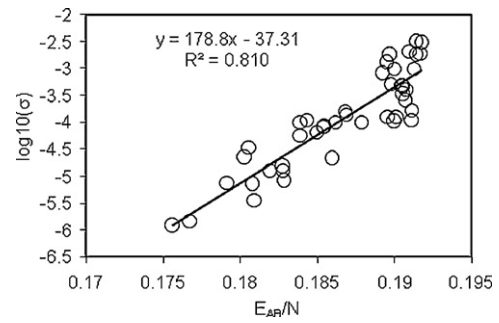


Fig. 3. Linear relationship between experimental ionic conductivities (in logarithmic form) and calculated nominal Coulomb energy of oxygen stoichiometric oxyapatites reported in literature.

$$E_{La}^{mod} = E_{La}^{org}(R_{La}^{org})^{0.6} \quad (21)$$

The charge densities of the A site and B site, i.e., ρ_A^{mod} and ρ_B^{mod} , are defined in terms of the modified electronegativities and the average charges, as shown in Eqs. (22) and (23), respectively. In particular, ρ_A^{mod} is defined as a standard density of unity minus a deviation from the electronegativity of La³⁺ when the A site is substituted with other cations. The deviation is normalized by the modified electronegativity of La³⁺ (E_{La}^{mod}) and averaged by the charge of A site (n_A^{avg}). ρ_B^{mod} is also defined in the similar way where the deviation from the standard density of unity is caused by the deviation of the B site from O²⁻. It is noted that the normalized deviation is multiplied by the factor of (9/4)² with 9 and 4 being the coordination numbers of La1/La2 and Si⁴⁺, respectively. Since positive Coulomb energy is taken into account, the absolute value of ρ_B^{mod} is used as shown in Eq. (23).

$$\rho_A^{mod} = 1 - \frac{E_A^{mod} - E_{La}^{mod}}{E_{La}^{mod}n_A^{avg}} \quad (22)$$

$$\rho_B^{mod} = \left| -1 + \frac{E_B^{mod} - E_O^{mod}}{E_O^{mod}n_B^{avg}} \left(\frac{9}{4}\right)^2 \right| \quad (23)$$

The re-defined radii in Eqs. (13) and (16) and charge densities in Eqs. (22)–(23) are substituted into Eq. (8c). By removing the constant γ , the relative Coulomb energy is obtained as defined by:

$$E_{AB}^{mod} = \frac{Z\rho_A^{mod}\rho_B^{mod}R_A^{avg}(R_B^{avg} + R_O^{org})}{\sqrt{(R_A^{avg})^2 + (R_B^{avg} + R_O^{org})^2 + d_{AB}^2}} \quad (8d)$$

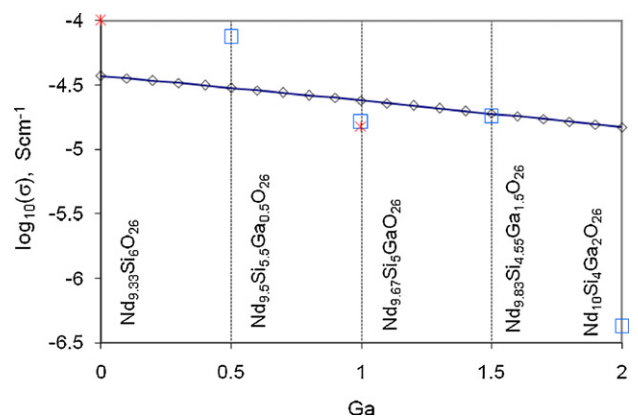


Fig. 4. Comparison of ionic conductivities of oxyapatites Nd_xSi_yGa_(6-y)O₂₆ obtained from model prediction (diamonds) and literature (squares from [24] and asterisks from [2,9]).

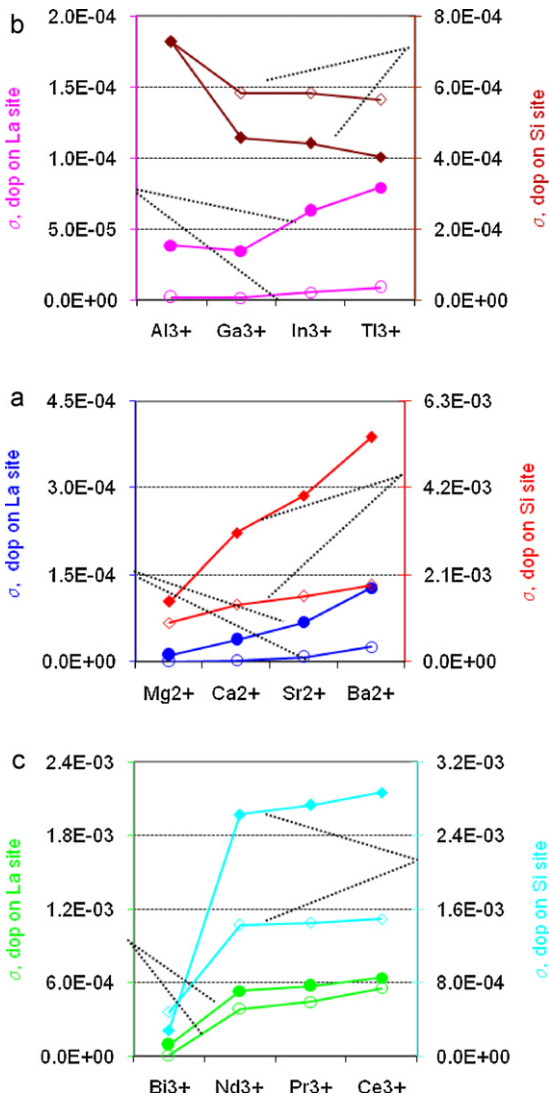


Fig. 5. Calculated ionic conductivity (S cm^{-1}) by doping M at La and Si sites. (a) $M = \text{Mg}^{2+}$, Ca^{2+} , Sr^{2+} , and Ba^{2+} (shaded circles— $\text{La}_{8.67}\text{MSi}_6\text{O}_{26}$, open circles— $\text{La}_9\text{M}_2\text{Si}_6\text{O}_{26}$, shaded diamonds— $\text{La}_{10}\text{Si}_5\text{MO}_{26}$, open diamonds— $\text{La}_{9.67}\text{Si}_{5.5}\text{M}_{0.5}\text{O}_{26}$); (b) $M = \text{Al}^{3+}$, Ga^{3+} , In^{3+} and Tl^{3+} (shaded circles— $\text{La}_{8.33}\text{MSi}_6\text{O}_{26}$, open circles— $\text{La}_{7.33}\text{M}_2\text{Si}_6\text{O}_{26}$, shaded diamonds— $\text{La}_{9.67}\text{Si}_5\text{MO}_{26}$, open diamonds— $\text{La}_{9.5}\text{Si}_{5.5}\text{M}_{0.5}\text{O}_{26}$); (c) $M = \text{Bi}^{3+}$, Nd^{3+} , Pr^{3+} and Ce^{3+} (shaded circles— $\text{La}_{8.33}\text{MSi}_6\text{O}_{26}$, open circles— $\text{La}_{7.33}\text{M}_2\text{Si}_6\text{O}_{26}$, shaded diamonds— $\text{La}_{9.67}\text{Si}_5\text{MO}_{26}$, open diamonds— $\text{La}_{9.5}\text{Si}_{5.5}\text{M}_{0.5}\text{O}_{26}$).

The relative Coulomb energy E_{AB}^{mod} is then correlated to the ionic conductivity σ . As shown in the following section, E_{AB}^{mod} is nearly linear to the logarithmic σ . It follows from the model that the larger the relative Coulomb energy, the higher the ionic conductivity. Furthermore, it is readily available to predict the ionic conductivity of oxyapatite electrolyte materials by using this model.

3. Results and discussion

3.1. Model validation

As shown in Eq. (8d), the inputs to the calculation of E_{AB}^{mod} are the fundamental element properties of ionic radii, electronegativities, and valences that can be found in [25,26]. Table 1 lists the fundamental data of the elements used in this study. The ionic conductivities of 45 reported oxyapatites at 500°C are summarized in Table 2 and are used to validate the developed model. The unknown

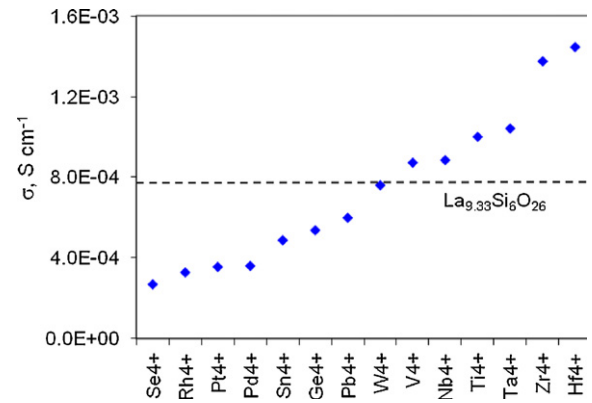


Fig. 6. Calculated ionic conductivity by substituting one tetravalent cation at Si site. General formula of oxyapatite is $\text{La}_{9.33}\text{Si}_5\text{MO}_{26}$ ($M = \text{M}^{4+}$).

universal constant λ , as introduced in Eq. (17), is given as 1, implying close contact of two charged units.

E_{AB}^{mod} is calculated and divided by the total number of cations for each sample listed in Table 2, and plotted against the logarithmic ionic conductivity (Fig. 3). A linear relation is found with the coefficient of the determination (R^2) of 0.81, which indicates a very good linear correlation.

The linear function is used to predict the ionic conductivity from the relative Coulomb energy. The predictive capability is examined by comparing the calculated ionic conductivities with the reported results [2,9,27] of five oxyapatites of the general formula $\text{Nd}_x\text{Si}_y\text{Ga}_{(6-y)}\text{O}_{26}$ ($y = 4-6$), as shown in Fig. 4. The results show that the ionic conductivities of these oxyapatites decrease as more Ga^{3+} cations are doped at the Si^{4+} site, and the predicted trend is in agreement with the literature data. While the ionic conductivities generated from the model decrease monotonously, the data reported in the literature fluctuate around the trend line, with the exception of that for $\text{Nd}_{10}\text{Si}_4\text{Ga}_2\text{O}_{26}$.

3.2. Effects of doping

In this section, the effects of doping cations on the changes of ionic conductivity are investigated based on the typical oxyapatite $\text{La}_{9.33}\text{Si}_6\text{O}_{26}$ by using the developed model. In particular, ionic conductivities predicted from doping cations of valence 2+, 3+ or 4+ on the La or Si sites are examined. Since the present study focuses on oxygen stoichiometric oxyapatites, the stoichiometry of the cations is adjusted accordingly to maintain the oxygen stoichiometry at 26 when incorporating dopants into the structure. In order to conduct a consistent study among all the predictions, the predicted ionic conductivity ($7.36 \times 10^{-4} \text{ S cm}^{-1}$) instead of the experimental ($1.1 \times 10^{-4} \text{ S cm}^{-1}$) of $\text{La}_{9.33}\text{Si}_6\text{O}_{26}$ is taken as the reference.

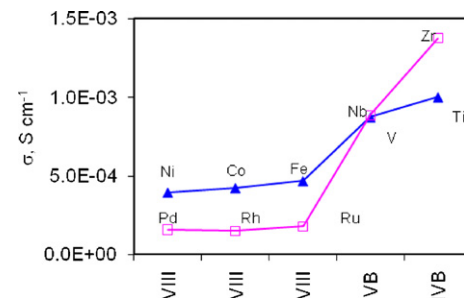


Fig. 7. Calculated ionic conductivity of oxyapatites $\text{La}_{9.67}\text{Si}_5\text{MO}_{26}$ ($M = 3+$) and $\text{La}_{9.33}\text{Si}_5\text{MO}_{26}$ ($M = 4+$) by doping M cations of 4th period (Ni, Co, Fe, V, Ti) and 5th period (Pd, Rh, Ru, Nb, Zr).

3.2.1. Doping at the La site

The effects of doping cations on the La site of $\text{La}_{9.33}\text{Si}_6\text{O}_{26}$ are studied with three simulated scenarios that correspond to doping three groups of cations, respectively, namely: (i) Mg^{2+} , Ca^{2+} , Sr^{2+} , and Ba^{2+} (Group IIA in the periodic table); (ii) Al^{3+} , Ga^{3+} , In^{3+} , and Tl^{3+} (Group IIIA in the periodic table); (iii) Bi^{3+} , Nd^{3+} , Pr^{3+} , and Ce^{3+} .

Doping divalent cations of Group (i) at the La site was first studied. Specifically, the incorporation of two levels of dopants M (Mg^{2+} , Ca^{2+} , Sr^{2+} , and Ba^{2+}) was investigated according to the formula $\text{La}_{8.67}\text{MSi}_6\text{O}_{26}$ and $\text{La}_8\text{M}_2\text{Si}_6\text{O}_{26}$. It is noted that the lower charge on M (2+) is balanced by an increased La content so that the oxygen content is maintained as nominally stoichiometric. As shown in Fig. 5a (shaded and open circles), all the calculated ionic conductivities (σ) are smaller than that of $\text{La}_{9.33}\text{Si}_6\text{O}_{26}$ when doping M^{2+} at the La site. Furthermore, samples with higher dopant levels result in lower σ values. For instance, the σ values of $\text{La}_8\text{M}_2\text{Si}_6\text{O}_{26}$ (open circles) are lower than those of $\text{La}_{8.67}\text{MSi}_6\text{O}_{26}$ (shaded circles). Such trends are in a good agreement with reported observations [3] which revealed that the magnitude of the change in σ to be strongly dependent on the size of the dopant cation, and that small dopants at the La site are detrimental to σ . This study showed that ionic size may not be the sole determining factor. For instance, the ionic radii (Å) of Mg^{2+} , Ca^{2+} , Sr^{2+} and Ba^{2+} are 0.72, 1, 1.18 and 1.35, respectively, while the ionic radius of La^{3+} (=1.03) is in between. The present study reveals that another factor, the electronegativity, also plays an important role. In fact, the coupling effect of ionic radius and electronegativity determines the resulting ionic conductivity via the relative Coulomb energy. The calculation shows that the Coulomb energy of $\text{La}_{9.33}\text{Si}_6\text{O}_{26}$ is 0.191, while the resultant relative Coulomb energies of $\text{La}_8\text{M}_2\text{Si}_6\text{O}_{26}$ are 0.172, 0.177, 0.180 and 0.183 for $\text{M} = \text{Mg}^{2+}$, Ca^{2+} , Sr^{2+} and Ba^{2+} , respectively, that is all values are below 0.191. Similarly, the Coulomb energies of $\text{La}_{8.67}\text{MSi}_6\text{O}_{26}$ ($\text{M} = \text{Mg}^{2+}$, Ca^{2+} , Sr^{2+} and Ba^{2+}) are also less than 0.191.

Similar to the first scenario, two levels of dopant contents were investigated for the second and third scenarios, respectively. The two dopant levels are represented by the general formula of $\text{La}_{8.33}\text{MSi}_6\text{O}_{26}$ and $\text{La}_{7.33}\text{M}_2\text{Si}_6\text{O}_{26}$. The calculated σ values of the second scenario are presented in Fig. 5b (shaded and open circles). The behavior of this group of trivalent cations is generally similar to that of the divalent cations in the first scenario, except that Ga^{3+} deviates slightly from the trend. The calculated σ values of the third scenario are shown in Fig. 5c (shaded and open circles). As seen in Fig. 5b and c, all the calculated σ values are lower than that of $\text{La}_{9.33}\text{Si}_6\text{O}_{26}$, and the larger doping content leads to a more significant decrease in σ . These results can be explained from the relative Coulomb energies of the samples in the two scenarios. For instance, the relative Coulomb energies of $\text{La}_{8.33}\text{MSi}_6\text{O}_{26}$ ($\text{M} = \text{Bi}^{3+}$, Nd^{3+} , Pr^{3+} and Ce^{3+}) are 0.1862, 0.1904, 0.1905 and 0.1908, respectively, all of which are smaller than that of $\text{La}_{9.33}\text{Si}_6\text{O}_{26}$. A further examination of the third scenario shows that the same trends as those of the first scenario are observed in the samples doped with Nd^{3+} , Pr^{3+} and Ce^{3+} . It is noted that the ionic radii of these three cations increase ($R_{\text{Nd}} < R_{\text{Pr}} < R_{\text{Ce}}$), while their electronegativities decrease ($E_{\text{Nd}} > E_{\text{Pr}} > E_{\text{Ce}}$). In the case of dopant Bi^{3+} , its ionic radius is the same as La^{3+} , but its electronegativity (1.9) is significantly larger than that of La^{3+} (1.1), which leads to the significant lower relative Coulomb energy of $\text{La}_{8.33}\text{BiSi}_6\text{O}_{26}$ (0.1862). This explains the dramatic reduction in σ of Bi-doped oxyapatites reported in [3]. Overall, doping at the La site leads to a reduction of ionic conductivity, but the dopants with large ionic radii and small electronegativities at the La site generally result in less decrease in ionic conductivity.

3.2.2. Doping at the Si site

In the same manner as Section 3.2.1, the effects of doping at the Si site of $\text{La}_{9.33}\text{Si}_6\text{O}_{26}$ were studied for five simulated scenarios.

In particular, Scenarios (1)–(3) focus on the same cations as those doped on the La site (see Section 3.2.1). Similarly, two different levels of dopant contents are calculated for each of the three scenarios and the results are plotted in Fig. 5a–c, respectively, in comparison with the results of Section 3.2.1. Doping tetravalent cations at the Si site is studied in Scenario (4), and doping trivalent and tetravalent cations standing in the 4th and 5th period in the periodic table is studied in Scenario (5).

The results of Scenario (1) are shown in Fig. 5a with two general formulae of $\text{La}_{10}\text{Si}_5\text{MO}_{26}$ (shaded diamonds) and $\text{La}_{9.67}\text{Si}_{5.5}\text{M}_{0.5}\text{O}_{26}$ (open diamonds). Doping at the Si site with Group IIA cations shows a steady boost in ionic conductivity, σ , and the higher level of dopants results in a larger increase in σ , which is similar to the trends of doping at the La site. In contrast to doping at the La site, however, all the calculated σ values are larger than that of $\text{La}_{9.33}\text{Si}_6\text{O}_{26}$ for all levels of dopants at the Si site. This finding also agrees well with the reported observation in [3].

The results of Scenario (2) are shown in Fig. 5b with two general formulae of $\text{La}_{9.67}\text{Si}_5\text{MO}_{26}$ (shaded diamonds) and $\text{La}_{9.5}\text{Si}_{5.5}\text{M}_{0.5}\text{O}_{26}$ (open diamonds). It is found that doping Group IIIA cations at the Si site results in trends that are opposite to those of doping at the La site, and the σ values of both levels of dopant contents are smaller than that of $\text{La}_{9.33}\text{Si}_6\text{O}_{26}$. On the other hand, as shown in Fig. 5c (Scenario 3), doping rare earths of Nd^{3+} , Pr^{3+} and Ce^{3+} leads to a boost in σ . The substitution of Bi^{3+} at the Si site, however, lowers the ionic conductivity which is similar to that at the La site.

In Scenario (4), the substitution of isovalent ions at the Si site with the general formula of $\text{La}_{9.33}\text{Si}_5\text{MO}_{26}$ is examined and the results are presented in Fig. 6. Two opposite effects are observed. Doping W^{4+} , V^{4+} , Nb^{4+} , Ti^{4+} , Ta^{4+} , Zr^{4+} and Hf^{4+} leads to an increase in σ , where as doping Se^{4+} , Rh^{4+} , Pt^{4+} , Pd^{4+} , Sn^{4+} , Ge^{4+} and Pb^{4+} reduces σ . While the ionic radii of all these cations in the two groups are nearly equal to each other, the electronegativities of the cations of the former group are obviously smaller than those of the latter group. The resultant relative Coulomb energies of the former group are therefore larger and those of the latter group are smaller than the Coulomb energy of $\text{La}_{9.33}\text{Si}_6\text{O}_{26}$.

The effects of doping at the Si site with trivalent and tetravalent cations are compared further in Scenario (5). Two types of oxyapatites are evaluated with general formulae of $\text{La}_{9.67}\text{Si}_5\text{MO}_{26}$ ($\text{M} = \text{Ni}^{3+}$, Co^{3+} , Fe^{3+} , Pd^{3+} , Rh^{3+} , Ru^{3+}) and $\text{La}_{9.33}\text{Si}_5\text{MO}_{26}$ ($\text{M} = \text{V}^{4+}$, Ti^{4+} , Nb^{4+} , Zr^{4+}). The results are presented in Fig. 7. Apparently, the ionic conductivities of oxyapatites doped with tetravalent cations are noticeably higher than those with trivalent cations. It is noted that the electronegativities of V, Ti, Nb and Zr are significantly smaller than those of Ni, Co, Fe, Pd, Rh and Ru, while the ionic radii of the tetravalent cations are slightly larger or equivalent to those of the trivalent cations. The coupling effect of these two properties leads to higher ionic conductivities in oxyapatites doped with tetravalent elements. In summary, the calculation shows that doping at the Si site with cations of larger ionic radii and smaller electronegativities generally results in more significant increases in ionic conductivity.

While the predicted results suggest that substitution of Ti for Si improves the ionic conductivity, it seems to contradict the observation reported in [3]. The reported low ionic conductivity of Ti-doped oxyapatite could be related to the presence of secondary phase [28].

3.2.3. Effect of ionic radius and electronegativity

It has been shown that the ionic conductivity of an oxyapatite is determined by the coupling effect of the ionic radii and the electronegativities of the constituents via the relative Coulomb energy. To have a better insight into the roles of the two types of fundamental property, simulation studies are performed by systematically varying the ionic radii of dopants in the range of 0.2–1.4 Å and

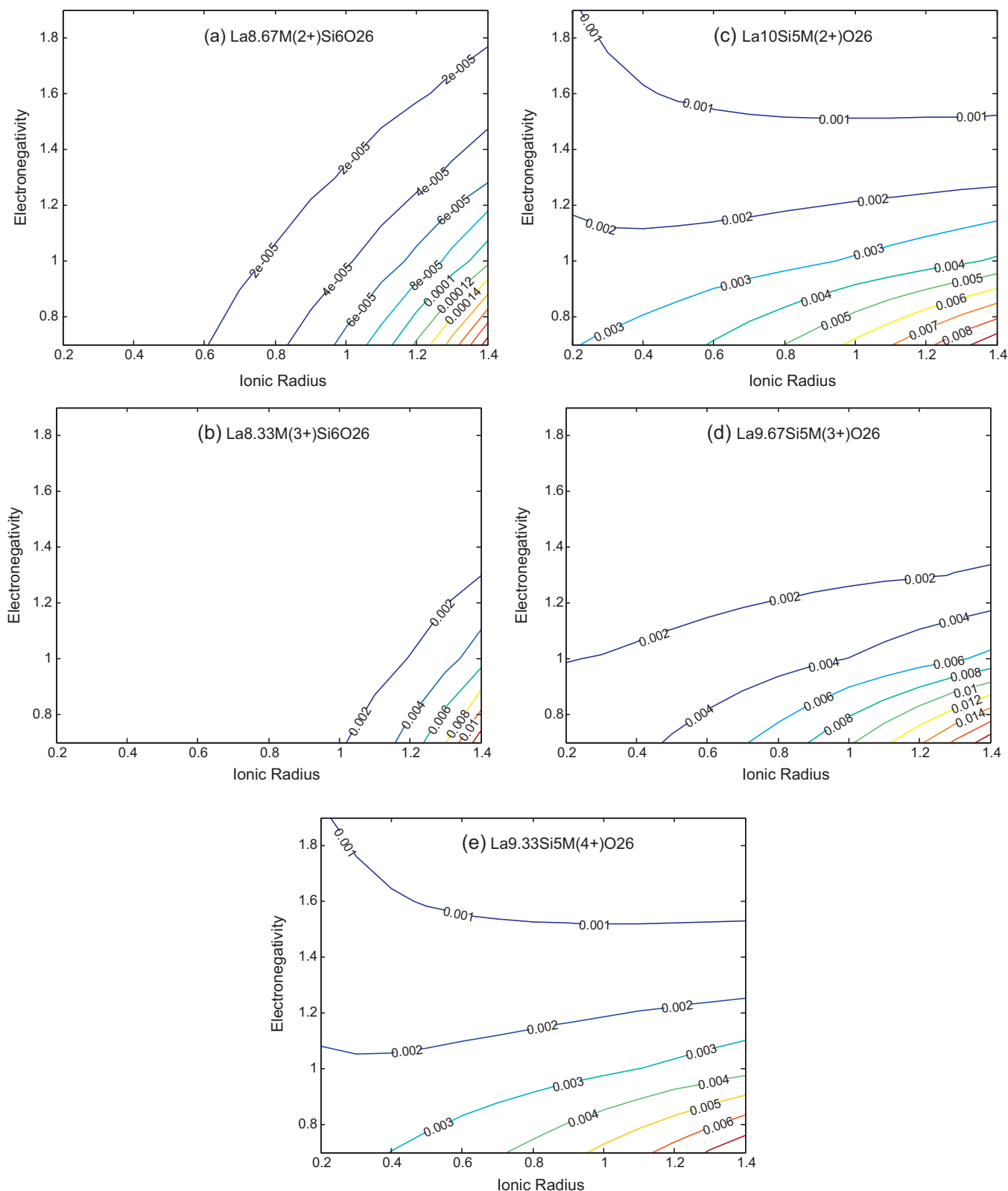


Fig. 8. Contour plots of ionic conductivity (S cm^{-1}) variation affected by ionic radius and electronegativity. (a) $\text{La}_{8.67}\text{MSi}_6\text{O}_{26}$ ($M=2+$), (b) $\text{La}_{8.33}\text{MSi}_6\text{O}_{26}$ ($M=3+$), (c) $\text{La}_{10}\text{Si}_5\text{MO}_{26}$ ($M=2+$), (d) $\text{La}_{9.67}\text{Si}_5\text{MO}_{26}$ ($M=3+$), (e) $\text{La}_{9.33}\text{Si}_5\text{MO}_{26}$ ($M=4+$).

electronegativities in 0.7–4. The study covered dopants of valence 2+ and 3+ at the La and Si sites, respectively, and valence 4+ at the Si site. By substituting one cation (denoted as M) into La or Si, five types of pseudo oxyapatite, namely, (a) $\text{La}_{8.67}\text{MSi}_6\text{O}_{26}$ ($M=2+$), (b) $\text{La}_{8.33}\text{MSi}_6\text{O}_{26}$ ($M=3+$), (c) $\text{La}_{10}\text{Si}_5\text{MO}_{26}$ ($M=2+$),

(d) $\text{La}_{9.67}\text{Si}_5\text{MO}_{26}$ ($M=3+$) and (e) $\text{La}_{9.33}\text{Si}_5\text{MO}_{26}$ ($M=4+$) are generated.

Five scenarios that are associated with the five types of oxyapatites are obtained and the contour plots are given in Fig. 8. A number of bands are observed in each plot and correspond to dif-

Table 3
Predicted ionic conductivity σ for new oxyapatites.

Type	Oxyapatite	σ (S cm ⁻¹)
A _{9.33} B ₆ O ₂₆ (A ³⁺ , B ⁴⁺)	Ce _{9.33} (Hf,Ta,Ti,Zr) ₆ O ₂₆	1.1 × 10 ⁻³ –8.7 × 10 ⁻³
	La _{9.33} (Hf,Nb,Ta,Ti,V,Zr) ₆ O ₂₆	1.7 × 10 ⁻³ –4.7 × 10 ⁻³
	Nd _{9.33} (Hf,Zr) ₆ O ₂₆	1.1 × 10 ⁻³ –1.5 × 10 ⁻³
	Pr _{9.33} (Hf,Zr) ₆ O ₂₆	2.1 × 10 ⁻³ –2.9 × 10 ⁻³
A ₁₀ B ₁₅ B ₂ O ₂₆ (A ³⁺ , B ¹⁴⁺ , B ²⁺)	Ce ₁₀ Hf ₅ (Ba,Ca,Sr) ₂ O ₂₆	1.7 × 10 ⁻² –2.7 × 10 ⁻²
	Ce ₁₀ Zr ₅ (Ba,Ca,Sr) ₂ O ₂₆	1.3 × 10 ⁻² –2.0 × 10 ⁻²
	La ₁₀ Hf ₅ (Ba,Ca,Sr) ₂ O ₂₆	6.8 × 10 ⁻² –1.1 × 10 ⁻¹
	La ₁₀ Hf ₅ (Co,Cu,Fe,Mg,Ni,V,Zr) ₂ O ₂₆	1.1 × 10 ⁻² –3.4 × 10 ⁻²
	La ₁₀ Ta ₅ (Ba,Ca,Sr) ₂ O ₂₆	1.2 × 10 ⁻² –2.0 × 10 ⁻²
	La ₁₀ Ti ₅ (Ba,Ca,Sr) ₂ O ₂₆	1.2 × 10 ⁻² –1.9 × 10 ⁻²
	La ₁₀ Zr ₅ (Ba,Ca,Sr) ₂ O ₂₆	5.1 × 10 ⁻² –8.1 × 10 ⁻²
	La ₁₀ Zr ₅ (Fe,Mg,V,Zr) ₂ O ₂₆	1.1 × 10 ⁻² –2.5 × 10 ⁻²
A ₂ B ₁₄ B ₂ O ₂₆ (A ³⁺ , B ¹⁴⁺ , B ²⁺)	Ce ₂ Hf ₄ (Ce,Dy,Er,Gd,Ho,La,Lu,Nd,Pr,Sm,Tb,Y,Yb) ₂ O ₂₆	1.0 × 10 ⁻² –3.7 × 10 ⁻²
	Ce ₂ Zr ₄ (Ce,Er,La,Lu,Nd,Pr,Sm,Tb,Yb) ₂ O ₂₆	1.1 × 10 ⁻² –2.9 × 10 ⁻²
	La ₂ Hf ₄ (Ce,Er,La,Lu,Tb,Yb) ₂ O ₂₆	8.2 × 10 ⁻² –1.5 × 10 ⁻¹
	La ₂ Hf ₄ (Dy,Er,Gd,Ho,Nd,Pr,Sm,Y) ₂ O ₂₆	3.9 × 10 ⁻² –7.6 × 10 ⁻²
	La ₂ Nb ₄ (Eu,La,Lu,Tb,Yb) ₂ O ₂₆	1.1 × 10 ⁻² –1.9 × 10 ⁻²
	La ₂ Si ₄ (Eu,La,Lu) ₂ O ₂₆	1.0 × 10 ⁻² –1.6 × 10 ⁻²
	La ₂ Ta ₄ (Ce,Dy,Er,Gd,Ho,La,Lu,Nd,Pr,Sm,Tb,Y,Yb) ₂ O ₂₆	1.0 × 10 ⁻² –3.9 × 10 ⁻²
	La ₂ Ti ₄ (Ce,Dy,Er,Gd,Ho,La,Lu,Nd,Pr,Sm,Tb,Y,Yb) ₂ O ₂₆	1.1 × 10 ⁻² –3.9 × 10 ⁻²
	La ₂ V ₄ (Ce,Er,La,Lu,Nd,Pr,Tb,Yb) ₂ O ₂₆	1.0 × 10 ⁻² –2.1 × 10 ⁻²
	La ₂ W ₄ Lu ₂ O ₂₆	1.0 × 10 ⁻²
	La ₂ Zr ₄ Lu ₂ O ₂₆	1.2 × 10 ⁻¹
	La ₂ Zr ₄ (Ce,Dy,Er,Er,Er,Gd,Ho,La,Nd,Pr,Sm,Tb,Y,Yb) ₂ O ₂₆	3.0 × 10 ⁻² –7.3 × 10 ⁻²
	Pr ₂ Hf ₄ Lu ₂ O ₂₆	1.2 × 10 ⁻²
	A _{9.33} B ₁₅ B ₂ O ₂₆ (A ³⁺ , B ¹⁴⁺ , B ²⁺)	La _{9.33} Hf ₅ (Ge,Nb,Pb,Si,Sn,Ta,Ti,V,W,Zr) ₂ O ₂₆
La _{9.33} Zr ₅ (Hf,Nb,Pb,Si,Ta,Ti,V,W) ₂ O ₂₆		1.0 × 10 ⁻² –2.6 × 10 ⁻²

ferent levels of ionic conductivity. The higher ionic conductivities are generally located at the lower right corners of the plots and are associated with larger radii and lower electronegativities. The ionic conductivities σ are essentially below 1 × 10⁻³ S cm⁻¹ when doping divalent cations at the La site (Fig. 8a). By contrast, doping trivalent cations leads to an increase in σ if the ionic radii are larger than 1 Å and electronegativities are smaller than 1.3 (Fig. 8b). For doping at the Si site (Fig. 8c–e), all the dopants of valence 2+, 3+ and 4+ enhance the ionic conductivities if their electronegativities are smaller than 1.3. In this case, the ionic radius is not a dominant factor, although a cation with larger ionic radius results in a higher σ .

3.3. Prediction of high ionic conductivity

In order to offer a guideline for the search of new oxyapatites with high ionic conductivities, the ionic conductivities for a wide range of pseudo oxyapatites are predicted by using the developed model. The new oxyapatites are virtually generated by numerically substituting a wide range of cations with valence of 2+, 3+, and 4+ into the La and Si sites, respectively. As mentioned above, doping divalent cations at the La site is detrimental, while doping trivalent cations can increase the ionic conductivity only if the ionic radius is larger than 1 Å and the electronegativity is smaller than 1.3 (as indicated in Fig. 8). Unfortunately, only a few trivalent cations meet such requirements. On the other hand, doping at the Si site is generally improves the conductivity. Therefore, four types of pseudo oxygen stoichiometric oxyapatite are generated with the general formula as (1) A_{9.33}B₆O₂₆ (A³⁺, B⁴⁺), (2) A₁₀B₁₅B₂O₂₆ (A³⁺, B¹⁴⁺, B²⁺), (3) A₁₀B₁₄B₂O₂₆ (A³⁺, B¹⁴⁺, B²⁺), and (4) A_{9.33}B₁₅B₂O₂₆ (A³⁺, B¹⁴⁺, B²⁺). In particular, the following cations are covered.

- A-site: Ce³⁺, Dy³⁺, Er³⁺, Eu³⁺, Gd³⁺, Ho³⁺, La³⁺, Lu³⁺, Nd³⁺, Pr³⁺, Sm³⁺, Tb³⁺, Y³⁺, Yb³⁺, B³⁺, Al³⁺, Ga³⁺, In³⁺, Tl³⁺, Bi³⁺.
- B1-site: Ge⁴⁺, Se⁴⁺, Si⁴⁺, Sn⁴⁺, Ta⁴⁺, Ti⁴⁺, V⁴⁺, W⁴⁺, Zr⁴⁺, Nb⁴⁺, Hf⁴⁺, Rh⁴⁺, Pt⁴⁺, Pd⁴⁺, Pb⁴⁺.

- B2-site: (a) divalent: Ba²⁺, Ca²⁺, Co²⁺, Cr²⁺, Cu²⁺, Fe²⁺, Mg²⁺, Mn²⁺, Mo²⁺, Ni²⁺, Pd²⁺, Sr²⁺, V²⁺, Zn²⁺; (b) trivalent: same cations as A-site; and (c) tetravalent: same cations as B1-site.

Since the number of such pseudo oxyapatites is very large, only those with calculated high ionic conductivities (at 500 °C) are selected and listed in Table 3. The ionic conductivities of type-1 (A_{9.33}B₆O₂₆) are the lowest (below 1 × 10⁻² S cm⁻¹) among the four types of oxyapatite. By contrast, the ionic conductivities of the other types are generally of the order of 10⁻² S cm⁻¹, and some of them are as high as 10⁻¹ S cm⁻¹. It is also found that La or Ce should be predominate at the A site in order to obtain high ionic conductivities. On the other hand, the substitution of Zr or Hf at the B site leads to the highest σ . To investigate the effect of doping levels of Zr at the Si site, the ionic conductivity of La_{9.33}Si_{6-y}Zr_yO₂₆ is calculated with y varying in the range of 0–6. The results are presented in Fig. 9. The ionic conductivity increases steadily with increasing the Zr⁴⁺ level. Furthermore, a significant increase in ionic conductivity occurs only when $y > 4$.

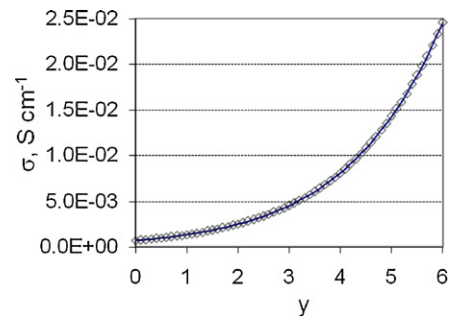


Fig. 9. Predicted ionic conductivity of La_{9.33}Si_{6-y}Zr_yO₂₆ with variation in doped Zr content.

4. Conclusions

It is demonstrated that two types of fundamental chemical property, i.e., electro-negativities and ionic radii of the constituents, control oxygen ionic conduction in oxyapatites. The two properties have been used to represent the relative charge densities and the distances between the charged units, respectively, and then to formulate the relative Coulomb energy. It is found that this relative Coulomb energy is linearly correlated to the oxygen ionic conductivity (in logarithmic form) in the oxyapatite systems. By applying the concept of the relative Coulomb energy, most experimentally observed trends can be well rationalized.

A wide range of new oxygen stoichiometric oxyapatites have been predicted with ionic conductivities in the order of 10^{-2} – 10^{-1} S cm⁻¹. Among them, lanthanum-based oxyapatites with Zr⁴⁺ or Hf⁴⁺ substituting for Si⁴⁺ have the highest ionic conductivities, which implies that this family of oxyapatites may be promising candidates for the electrolyte in IT-SOFCs. The prediction also shows that the substitution of Ta⁴⁺, Ti⁴⁺, Nb⁴⁺, W⁴⁺ and V⁴⁺ for Si⁴⁺ and the substitution of Ce³⁺ for La³⁺ results in relatively higher ionic conductivities. Finally, this study reveals that doping a cation with large ionic radius and low electro-negativity tends to increase the ionic conductivity of the oxyapatite. While these results are required to be verified by experiments, they offer a guideline in searching for promising oxyapatites with high ionic conductivities.

References

- [1] L. León-Reina, E.R. Losilla, M. Martínez-Lara, S. Bruque, M.A.G. Aranda, *J. Mater. Chem.* 14 (2004) 1142–1149.
- [2] P.R. Slater, J.E.H. Sansom, J.R. Tolchard, *Chem. Rec.* 4 (2004) 373–384.
- [3] E. Kendrick, M.S. Islam, P.R. Slater, *J. Mater. Chem.* 17 (2007) 3104–3111.
- [4] A. Najib, J.E.H. Sansom, J.R. Tolchard, P.R. Slater, M.S. Islam, *Dalton Trans.* (2004) 3106–3109.
- [5] S. Chefi, A. Madani, H. Boussetta, C. Roux, A. Hammou, *J. Power Sources* 177 (2008) 464–469.
- [6] J.E.H. Sansom, P.R. Slater, *Annu. Rep. Prog. Chem., Sect. A* 101 (2005) 489–512.
- [7] L. León-Reina, E.R. Losilla, M. Martínez-Lara, M.C. Martín-Sedenño, S. Bruque, P. Nuñez, D.V. Sheptyakov, M.A.G. Aranda, *Chem. Mater.* 17 (2005) 596–600.
- [8] J. McFarlane, S. Barth, M. Swaffer, J.E.H. Sansom, P.R. Slater, *Ionics* 8 (2002) 149–154.
- [9] J.E.H. Sansom, E. Kendrick, J.R. Tolchard, M.S. Islam, P.R. Slater, *J. Solid State Electron.* 10 (2006) 562–568.
- [10] A.L. Shaula, V.V. Kharton, M.V. Patrakeev, J.C. Waerenborgh, D.P. Rojas, N.P. Vyshatko, E.V. Tsipis, A.A. Yaremchenko, F.M.B. Marques, *Mater. Res. Bull.* 39 (2004) 763–773.
- [11] A.A. Yaremchenko, A.L. Shaula, V.V. Kharton, J.C. Waerenborgh, D.P. Rojas, M.V. Patrakeev, F.M.B. Marques, *Solid State Ionics* 171 (2004) 51–59.
- [12] L. León-Reina, J.M. Porras-Vázquez, E.R. Losilla, M.A.G. Aranda, *Solid State Ionics* 177 (2006) 1307–1315.
- [13] E.J. Abram, C.A. Kirk, D.C. Sinclair, A.R. West, *Solid State Ionics* 176 (2005) 1941–1947.
- [14] E. Beichade, I. Julien, T. Iwata, O. Masson, P. Thomas, E. Champion, K. Fukuda, *J. Eur. Ceram. Soc.* 28 (2008) 2717–2724.
- [15] F.M.B. Marques, V.V. Kharton, E.N. Naumovich, A.L. Shaula, A.V. Kovalevsky, A.A. Yaremchenko, *Solid State Ionics* 177 (2006) 1697–1703.
- [16] H. Yoshioka, S. Tanase, *Solid State Ionics* 176 (2005) 2395–2398.
- [17] S. Nakayama, M. Sakamoto, *J. Eur. Ceram. Soc.* 18 (1998) 1413–1418.
- [18] E.J. Abram, D.C. Sinclair, A.R. West, *J. Mater. Chem.* 11 (2001) 1978–1979.
- [19] J.E.H. Sansom, D. Richings, P.R. Slater, *Solid State Ionics* 139 (2001) 205–210.
- [20] J.R. Tolchard, M.S. Islam, P.R. Slater, *J. Mater. Chem.* 13 (2003) 1956.
- [21] E. Kendrick, M.S. Islam, P.R. Slater, *Solid State Ionics* 177 (2007) 3411–3416.
- [22] M.S. Islam, J.R. Tolchard, P.R. Slater, *Chem. Commun.* 9 (2003) 1486–1487.
- [23] E. Kendrick, J.E.H. Sansom, J.R. Tolchard, M.S. Islam, P.R. Slater, *Faraday Discuss.* 134 (2007) 181–194.
- [24] S. Beaudet-Savignat, A. Vincent, S. Lambert, F. Gervais, *J. Mater. Chem.* 17 (2007) 2078–2087.
- [25] D. Lide, *CRC Handbook of Chemistry and Physics*, 87th ed., CRC Press, Cleveland, OH, 1977, Ionic radius: http://en.wikipedia.org/wiki/Ionic_radius.
- [26] P. Sillars, F. Hulliger, *J. Less Common Met.* 132 (1987) 289–315, Boron Element Facts, <http://www.chemicool.com/elements/boron.html>; Europium Element Facts, <http://www.chemicool.com/elements/europium.html>.
- [27] J.R. Tolchard, J.E.H. Sansom, M.S. Islam, P.R. Slater, *Ionics* 10 (2004) 353–357.
- [28] J.E.H. Sansom, P.A. Sermon, P.R. Slater, *Solid State Ionics* 176 (2005) 1765–1768.